Atmospheric Research 307 (2024) 107481

Contents lists available at ScienceDirect

Atmospheric Research

journal homepage: www.elsevier.com/locate/atmosres

Multi-model ensemble bias-corrected precipitation dataset and its application in identification of drought-flood abrupt alternation in China

Tingting Liu [a,b], Xiufang Zhu [a,b,*], Mingxiu Tang [a,b], Chunhua Guo [a,b], Dongyan Lu [a,b]

[a] Key Laboratory of Environmental Change and Natural Disaster, Ministry of Education, Beijing Normal University, Beijing 100875, China
[b] Institute of Remote Sensing Science and Engineering, Faculty of Geographical Science, Beijing Normal University, Beijing 100875, China.

ARTICLE INFO

Keywords:
Precipitation dataset
DFAA
EQM

ABSTRACT

High precision precipitation products are the basis of precipitation-related research. Based on 27 global climate models (GCMs) in the Coupled Model Intercomparison Project phase 6 (CMIP6), we designed eight schemes for comprehensively using the empirical quantile mapping (EQM) method and data ensemble method to conduct precipitation bias correction; then, we selected the scheme with the highest accuracy as the final bias correction scheme. Using the selected bias correction scheme, we created a monthly precipitation dataset with a 1° spatial resolution, which spans the historical period of 1961–2014 and the future period of 2015–2099 under three shared socioeconomic pathway (SSP) scenarios: SSP126, SSP245, and SSP585. The corrected precipitation data were validated using the CN05.1 grid precipitation dataset from the China Meteorological Data Sharing Network and were compared with the ERA5 precipitation data from the European Centre for Medium-Range Weather Forecasts. The dataset was also utilized for future prediction of alternating drought and flood events in China. The results show that this best bias correction scheme is the first to integrate precipitation simulation data from 27 GCMs using the random forest (RF) model and then the EQM method to further correct the integrated precipitation data. The corrected precipitation data are better than the original GCM precipitation data in terms of both the monthly precipitation and extreme precipitation. From the perspective of the monthly precipitation, the difference between the ERA5 and RF-EQM is small, but the extreme precipitation of the RF-EQM clearly outperforms the ERA5 extreme precipitation. For the annual maximum (minimum) monthly precipitation, the correlation coefficient, the RMSD (standardized), and the STD (standardized) between the ERA5 and CN05.1 are 0.925 (0.743), 0.474 (1.223), and 1.207 (1.765), respectively; the correlation coefficient, the RMSD (standardized), and the STD (standardized) between the RF-EQM and CN05.1 are 0.947 (0.735), 0.337 (0.837), and 0.849 (1.226), respectively. The occurrence frequency of DF (an abrupt change from drought to flood) events is continuously increasing in all scenarios, with the highest frequency observed under the SSP585 scenario. The increase in FD (an abrupt change from flood to drought) event frequency is not pronounced. This study expands the method for bias correction of meteorological data and provides a reference for other climate parameters and precipitation bias correction in other regions.

1. Introduction

Precipitation is a key meteorological and climatic parameter (Kukulies et al., 2020; Michelson, 2004; Morin et al., 2020), with spatial distribution having a certain impact on meteorological, hydrological, and related processes (Baez-Villanueva et al., 2020; Chen and Chung, 2015; Gat and Airey, 2006; Niu et al., 2017). Changes in precipitation affect agriculture, animal husbandry, hydropower, and water conservancy (Mukhamedjanov et al., 2021; Seo and Mendelsohn, 2008; Tabari, 2020; Wei et al., 2020). Therefore, obtaining reliable and accurate precipitation data is of great significance for analyzing and predicting hydrological processes, allocating and managing water resources, and predicting drought and flood disasters.

Global climate models (GCMs) have been widely used in related research on the impact of past, present, and future climate changes (Taylor et al., 2012; Fu et al., 2013; Huang et al., 2014; Ta et al., 2018; Jiang et al., 2020a; Guo et al., 2021; Jiang and Zhou, 2021; Yao et al., 2021). The Coupled Model Intercomparison Project (CMIP) has now

* Corresponding author at: Key Laboratory of Environmental Change and Natural Disaster, Ministry of Education, Beijing Normal University, Beijing 100875, China.
E-mail address: zhuxiufang@bnu.edu.cn (X. Zhu).

https://doi.org/10.1016/j.atmosres.2024.107481
Received 2 February 2024; Received in revised form 21 April 2024; Accepted 15 May 2024
Available online 21 May 2024

reached its sixth phase (CMIP6). The number of GCMs included in the project has increased with each successive phase, and the resolution of the GCMs has improved. Compared with the CMIP3 and CMIP5, the performances of the GCMs in CMIP6 are significantly better (Chen et al., 2020a, 2021; Gusain et al., 2020; Jiang et al., 2020b; Wang et al., 2020; Wu et al., 2019; You et al., 2021; Harvey et al., 2020; Cannon, 2020; He et al., 2019; Xin et al., 2020; Fernandez-Granja et al., 2021; Bock et al., 2020; Zhu et al., 2020). In general, the GCMs can effectively reflect large-scale climate conditions, but they have limitations in describing regional climate processes and cannot be directly used in regional climate prediction and impact research. To solve this problem, we need to correct the bias of the GCMs' simulation data.

In recent years, GCM bias correction has become an important research topic. GCM bias correction includes the correction of the mean, variance, and quantile of the data. Relevant research has shown that the performance of quantile mapping bias correction is better than those of the bias correction methods that only correct the mean or the mean and variance of the precipitation data series (Gudmundsson et al., 2012; Taylor et al., 2012; Chen et al., 2013). Many studies have used quantile mapping to correct the bias of GCM data (Supharatid et al., 2022; Song et al., 2021; Lim Kam Sian et al., 2022; Shrestha et al., 2020; Piao et al., 2022; Xiang et al., 2022; Oruc, 2022; Babaousmail et al., 2022). Jose and Dwarakish (2022) used six bias correction methods, including the delta change (DC), linear scaling (LS), empirical quantile mapping (EQM), adjusted quantile mapping (AQM), Gamma-Pareto quantile mapping (GPQM), and quantile delta mapping (QDM) methods, to correct temperature data for the Netravati Basin in India. Their results demonstrate that these methods can significantly reduce data bias, except for the LS method. Li et al. (2010) developed the equidistant cumulative distribution function (EDCDF) method to adjust the cumulative distribution function (CDF) of model predictions based on the differences between the model outputs and observations in historical periods. The EDCDF method is very efficient in reducing model deviation (Yang et al., 2018; Sachindra et al., 2014) but does not have an ideal effect on simulating the precipitation field; EDCDF also produces a negative precipitation bias after correction. Based on the EDCDF method, Wang and Chen (2014b) proposed the equi-ratio cumulative distribution function (ERCDF) method. The ERCDF can solve the problem that the negative bias of the corrected precipitation produced by the EDCDF method (Wang and Chen, 2014; Baran et al., 2019); however, it cannot retain the dependence between the variables and introduces additional errors in the spatial gradient of the variables (Colette et al., 2012; White and Toumi, 2013). In addition, the ERCDF was developed for the correction of a single model dataset, and the uncertainty of a single model dataset can be large.

In recent years, some studies have also used methods based on a multi-model ensemble for bias correction, but often only a simple arithmetic average is used to achieve the fusion of multi-model data. Compared with single-model data, the accuracy of the multi-model ensemble results is improved, but the results of the multi-model ensemble based on a simple arithmetic average reduce the ability to capture extreme weather events to a certain extent. Some studies have optimized the multi-model ensemble based on a simple arithmetic average. For example, Zarrin et al. (2022) used the independent weighted mean method to assemble precipitation data for Iran from five GCMS and significantly improved the reliability of the simulation results. Several studies have combined the quantile mapping and multi-model ensemble methods to correct the bias of GCM data (Li et al., 2020a; Xu et al., 2021; Carvalho et al., 2021; Dike et al., 2022; Mondal et al., 2021). For example, Yue et al. (2021) and Supharatid et al. (2021) took China and Southeast Asia as their study areas, respectively. First, the single GCM simulation data were corrected using the empirical quantile mapping method; then, the outputs of the empirical quantile mapping method were fused using the mean based multi-model ensemble (MME) bias correction method. Song et al. (2022) first used the quantile mapping (QM) method to correct the bias of 11 GCM datasets, then used the technique for order preference by similarity to ideal solution (TOPSIS) method to determine the weights of the 11 corrected GCM dataset, and obtained the final correction result via weighted summation. However, the number of GCMs used in this study was small, and the results of the TOPSIS method are heavily dependent on the selected evaluation index, leading to some uncertainty. In recent years, some studies have employed machine learning methods for multi-model integration of GCM data (Ahmed et al., 2020; Wang et al., 2018; Dey et al., 2022; Jose et al., 2022). Li et al. (2021a, 2021b) utilized three methods, namely arithmetic mean, linear regression, and random forest, for multi-model integration of temperature and precipitation data in China, demonstrating the superiority of the random forest approach in this work. Yang et al. (2022) compared the application effects of decision tree algorithm, random forest algorithm, and adaptive boosting algorithm in the multi-model integration of precipitation data in China. The results indicated that the random forest algorithm had the smallest error. However, this study only employed four model datasets and did not incorporate bias correction methods. Shetty et al. (2023) applied the EQM for calibration of 13 GCM model datasets, followed by the utilization of eight methods for multi-model data integration. Nevertheless, this study employed a relatively limited number of models and did not evaluate extreme precipitation events. Currently, the use of machine learning methods for multi-model integration often faces challenges such as a limited number of GCMs, lack of incorporation of bias correction methods, and insufficient consideration of extreme precipitation events. Due to the impact of large-scale climate variability, precipitation in China is vulnerable to climate change (Held and Soden, 2006). In addition, China's complex terrain also increases the uncertainty of China's precipitation. Several studies have conducted bias correction on China's precipitation data, but these studies tended to focus on local areas of China or only focused on the applicability of the correction method to the monthly precipitation, without paying attention to the ability of the correction method to capture extreme precipitation events.

In summary, taking China as the research area, we designed eight fusion correction schemes by comprehensively using the empirical quantile mapping method and data ensemble method, corrected and assembled all of the available GCM simulated precipitation datasets in the CMIP6, compared the accuracy of the multi-model ensemble precipitation products obtained from the eight schemes, and selected the scheme with the highest accuracy. Using the selected scheme, we produced a monthly precipitation fusion product corrected for China with 1° spatial resolution from January 1961 to December 2099 using the multi-model ensemble (MME) bias correction method. The product satisfactorily reflects both the average state of the precipitation and extreme precipitation events. The future precipitation dataset produced in this study provides basic data for research on future precipitation-related events and can also be used as input data for dynamic downscaling models to improve the reliability of future precipitation-related research.

2. Data

The data used in this study included monthly precipitation data from 1961 to 2014 from the CN05.1 gridded dataset, monthly simulated precipitation data from 27 GCMs in the CMIP6 (detailed information can be found in Table 1) for historical and future periods (1961–2099), and the ERA5 reanalysis monthly precipitation summary dataset for 1979–2014.

The CN05.1 gridded dataset was obtained from the China Meteorological Data Sharing Network and was used as the observation data (Wu and Gao, 2013), with a resolution of 0.25° × 0.25°. This dataset was produced via interpolation of precipitation observations at 2416 National Meteorological Center stations in China (New et al., 2002; Xie et al., 2007). All CN05.1 grid data files have undergone strict quality inspection control, data verification, data correction, and

Table 1
Basic information about the GCMs used in this study.

Model	Country	Resolution (longitude× latitude)	Model	Country	Resolution (longitude× latitude)
ACCESS-CM2	Australia	1.675° × 1.25°	GFDL-ESM4	United States	1.25° × 1°
ACCESS-ESM1–5	Australia	1.875° × 1.25°	IITM-ESM	India	1.875° × 1.875°
AWI-CM-1-1-MR	Germany	0.9375° × 0.9375°	INM-CM4–8	Russia	2° × 1.5°
BCC-CSM2-MR	China	1.125° × 1.125°	INM-CM5–0	Russia	2° × 1.5°
CAMS-CSM1–0	China	1.125° × 1.1125°	IPSL-CM6A-LR	France	2.5° × 1.26°
CanESM5	Canada	2.8125° × 2.8125°	KACE-1-0-G	Korea	1.875° × 1.25°
CAS-ESM2–0	China	1.406° × 1.389°	KIOST-ESM	Korea	1.875° × 1.875°
CESM2-WACCM	United States	1.25° × 0.9375°	MIROC6	Japan	1.406° × 1.389°
CMCC-CM2-SR5	Italy	1.25° × 0.9375°	MPI-ESM1–2-HR	Germany	0.9375° × 0.9375°
CMCC-ESM2	Italy	1.25° × 0.9375°	MRI-ESM2–0	Japan	1.125° × 1.124°
EC-Earth3	10 European countries	0.703° × 0.703°	NESM3	China	1.875° × 1.865°
EC-Earth3-Veg	10 European countries	0.703° × 0.703°	NorESM2-MM	Norway	1.25° × 0.9375°
FGOALS-f3-L	China	1.25° × 1°	TaiESM1	China	1.25° × 0.9375°
FIO-ESM-2-0	China	1.25° × 0.9424°			

Note: The temporal resolution of the model data in the table is month, and the data used is from China.

supplementary recording, and have been widely recognized and applied in China. The CN05.1 has been widely used for verifying and correcting GCM simulations in China in relevant research (Yi-Yang et al., 2021; Zhu et al., 2021; Dong et al., 2015; Yang et al., 2020). The CN05.1 precipitation data from 1961 to 1994 were used as the training set to build the bias correction models, and the data from 1995 to 2014 were used as the validation data to evaluate the accuracy of the corrected precipitation data.

The GCM data were obtained from the CMIP6 models (https://esgf-node.llnl.gov/projects/cmip6). The basic information about the GCMs is presented in Table 1. The GCM data from 1961 to 2014 were used to train the bias correction models, and the GCM data from 2015 to 2099 under three shared socioeconomic pathway (SSP) scenarios (SSP126, SSP245, and SSP585) were used to produce the corrected future precipitation data. Because the spatial resolution of each GCM is different, before the correction, bilinear interpolation was conducted to uniformly interpolate all of the GCM data to 1° × 1°.

The ERA5 data were obtained from the European Centre for Medium-Range Weather Forecasts (ECMWF). The ERA5 is the fifth-generation reanalysis product launched by the ECWMF after the ERA-Interim, and it provides a large number of marine climate and hourly climate variables. The ERA5 has a resolution of 0.25° × 0.25° and provides a large number of hourly atmospheric, land, and marine climate variables. Significantly, ERA5 data's enhanced temporal and spatial resolution has been widely acknowledged in various studies, establishing it as a preferred tool for global climate research (Zou et al., 2022; Wang et al., 2022). Additionally, its ability to accurately depict annual and seasonal precipitation patterns in China has been demonstrated, albeit with a slight overestimation during summer months (Jiao et al., 2021). Here, the ERA5 reanalysis monthly precipitation data for 1979–2014 were used as the comparison data to assess the differences between the corrected precipitation data, ERA5 precipitation data, and reference precipitation data (CN05.1). Before conducting the comparison, we used bilinear interpolation to uniformly interpolate all of the GCMs of the ERA5 data to 1° × 1°.

3. Methods

3.1. Quantile mapping method

The EQM method uses the transfer function to correct the distribution of simulation data to match the distribution of the observation dataset (Déqué, 2007). This method uses the empirical nonparametric CDF without any assumptions about the precipitation distribution. The specific calculation formula is as follows:

$$P_{BC} = F_{obs}^{-1}(F_{sim}(x)),$$

where P_{BC} is the simulated precipitation after bias correction; F_{sim} is the CDF of the simulated data; F_{obs}^{-1} is the inverse function of the CDF of the observed data; and x is the simulated precipitation value of the GCM.

3.2. Ensemble methods

In this study, four GCM ensemble methods were used for the comparison, including the average, independent weighted mean, kernel density function, and random forest methods.

The average method is the most widely used GCM ensemble method. It directly averages the GCM data to achieve the fusion of multi-model data. This method has simple calculations, does not require a training dataset, and has been widely used in related research (Yue et al., 2021; Li et al., 2020b; Xu et al., 2021; Song et al., 2022; Lovino et al., 2021).

The purpose of the independent weighted mean (IWM) method is to find the linear fit of the model simulations that minimizes the mean square deviation (MSD) relative to the observations (Bai et al., 2021; Bishop and Abramowitz, 2013; Zarrin and Dadashi-Roudbari, 2021). More details about this method have been described by Bai et al. (2021).

Nonparametric kernel density estimation (KDE) is a nonparametric estimation method and can obtain the probability density function of data without prior knowledge (Sheather, 2004).

$$f(P) = \frac{1}{nh}\sum_{i=1}^{n} K\left(\frac{P - P_i}{h}\right),$$

where $f(\bullet)$ is the probability density function of the precipitation data of each model in a given grid within a pre-determined period; n is the number of samples (27 GCMs were used in this study, so $n = 27$); h is the window width; $K(\bullet)$ is a kernel function; and P is precipitation.

The kernel function is a weighting function or smoothing function. The common kernel functions are the Gaussian kernel function, Epanechnikov kernel function, triangular kernel function, and quartic kernel function. Relevant research has shown that the smaller the sample size of the data used is, the greater the possibility that the Gaussian kernel function is optimal (Scott, 1992; Duda et al., 2001). Because the sample size in this study was only 27, the Gaussian kernel function was used to calculate the probability density function. Based on the calculated probability density function, we calculated the precipitation value with the highest occurrence probability and took it as the precipitation value corrected using the kernel density function method.

The random forest regression model is a supervised ensemble statistical learning algorithm (Breiman, 2001). The random forest model is composed of multiple regression trees, and each decision tree is independent of the others. The final output of the model is determined by all of the decision trees. The random forest regression model mainly includes the following steps. First, the original data training sample set is recorded as A, and a new A_1, A_2, …, A_m sub-training set is obtained by

randomly extracting m sample points from training sample set A. Second for each sub-training set, a classification and regression tree (CART) is trained. In the training process, the segmentation rule for each node is to randomly select k features from all of the features, to select the optimal segmentation point from the k features, and then to divide the tree into the left and right subtrees. 3) Through the second step, many CARTs can be generated $f(A_1), f(A_2), \ldots, f(A_m)$, and the final prediction result is the average of all of the CART prediction results. The random forest model used in this study was built using the sklearn package in Python, and the gridsearchcv program was used to select the optimal parameters.

3.3. Design and optimal selection of bias correction scheme

In this study, we designed eight schemes for comprehensively using the EQM method and data ensemble method to conduct a precipitation bias correction, and we selected the scheme with the highest accuracy as the final bias correction scheme. The eight schemes were as follows: empirical quantile mapping followed by the multi-model ensemble method based on the simple arithmetic average method (EQM-Mean), empirical quantile mapping followed by independent weighted mean method (EQM-IWM), empirical quantile mapping followed by the kernel density function method (EQM-KDE), empirical quantile mapping followed by the random forest method (EQM-RF), the multi-model ensemble based on the simple arithmetic average method followed by empirical quantile mapping (Mean-EQM), the independent weighted mean method followed by empirical quantile mapping (IWM-EQM), the kernel density function method followed by empirical quantile mapping (KDE-EQM), and the random forest method followed by empirical quantile mapping (RF-EQM).

For each bias correction scheme, we used the CN05.1 data from 1961 to 1994 as the training set and the data from 1995 to 2014 as the validation set. The verified precipitation data included the monthly precipitation, annual maximum monthly precipitation, and annual minimum monthly precipitation. The validation indexes included the Pearson correlation coefficient, root mean square error (RMSE), mean absolute error (MAE), and comprehensive evaluation index M_s (Table 2) (Schuenemann and Cassano, 2009). The scheme with the highest M_s was used to produce a monthly precipitation fusion product under three climate scenarios (SSP126, SSP245, and SSP585) for January 2015 to December 2099.

Table 2
Validation indexes.

Statistical indicators	Calculation equations	Value range	Optimal value
Pearson correlation coefficient (R)	$R = \frac{\sum_{i=1}^{N}(E_i-\overline{E})(G_i-\overline{G})}{\sqrt{\sum_{i=1}^{N}(E_i-\overline{E})^2\sum_{i=1}^{N}(G_i-\overline{G})^2}}$	[−1,1]	1
Normalized Root mean square error (NRMSE)	$\mathrm{NRMSE} = \frac{1}{\overline{G}}*\sqrt{\frac{\sum_{i=1}^{N}(E_i-G_i)^2}{N}}$	[0, + ∞]	0
Mean absolute error (MAE)	$\mathrm{MAE} = \frac{\sum_{i=1}^{N}\lvert E_i-G_i\rvert}{N}$	[0, + ∞]	0
Comprehensive evaluation index (M_s)	$M_s = 1-\frac{\sum_{i=1}^{m} rank_i}{1\times m\times n}$	[0,1]	1

Note: N is the number of samples; E_i is the precipitation after bias correction; $\overline{E}$ is the average value of the corrected precipitation; G_i is the precipitation value from the CN05.1; $\overline{G}$ is the average value of precipitation from the CN05.1; n is the number of correction schemes (n =8); m is the total number of validation indexes (m=9, three validation indexes for each precipitation parameter, and three precipitation parameter, i.e., the monthly precipitation, annual maximum monthly precipitation, and annual minimum monthly precipitation); and $rank_i$ is the rank of the corrected GCM precipitation under the ith evaluation index. R, NRMSE and M_s are dimensionless, and MAE is in mm/month.

3.4. Identification of DFAA events based on the corrected precipitation data

This study employs the Standardized Precipitation Index (SPI) to quantify variations in floods and droughts (McKee et al., 1993). The Standardized Precipitation Index (SPI) is an indicator that characterizes the probability of precipitation occurrence, and it uses Γ probability distribution to describe the distribution of precipitation, and then normalized to obtain the SPI value, which is suitable for drought monitoring and evaluation on a monthly or above scale. Droughts and floods are common natural disasters (Bruce, 1994; Zhou et al., 2002). Drought-flood abrupt alternation (DFAA) refers to the alternating occurrence of drought and flood events within a short period (Wu et al., 2006; Shan et al., 2018; Chen et al., 2020b; Shi et al., 2021), usually resulting from the complex interplay between drought and heavy rainfall, forming compound events (Chen et al., 2020b). While adequate precipitation can alleviate drought (Chen et al., 2020a), the abrupt alternation between drought and flood can cause more severe damage than individual disaster. In this research, as shown in Fig. 1, DFAA events are defined from a perspective of event compounds, signifying abrupt transitions between drought (SPI ≤ -0.5) and flood (SPI ≥ 0.5) conditions in consecutive months (Chinese Academy of Meteorological Sciences, National Meteorological Center, Division of Disaster Prediction and Mitigation, Chinese Academy of Meteorological Sciences 2017). As shown in the figure, two types of DFAA events are defined in this paper: (1) an abrupt change from drought to flood (DF); (2) an abrupt change from flood to drought (FD).

4. Results

4.1. Selection of bias correction scheme

The evaluation results of the eight bias correction schemes are shown in Table 3. Regarding the monthly precipitation, the EQM-RF had the highest correlation coefficient with the CN05.1, and the lowest MAE and NRMSE values. Regarding the annual maximum monthly precipitation, the correlation coefficient between the EQM-Mean and CN05.1 was the highest performance, and the MAE and NRMSE values between the RF-EQM and CN05.1 were the lowest performance. Regarding the annual minimum monthly precipitation, the EQM-Mean had the highest correlation coefficient with the CN05.1, and the MAE and NRMSE values between the Mean-EQM and CN05.1 were the lowest performance. According to the comprehensive evaluation index M_s, the RF-EQM was the best correction method. Therefore, the RF-EQM was selected to produce

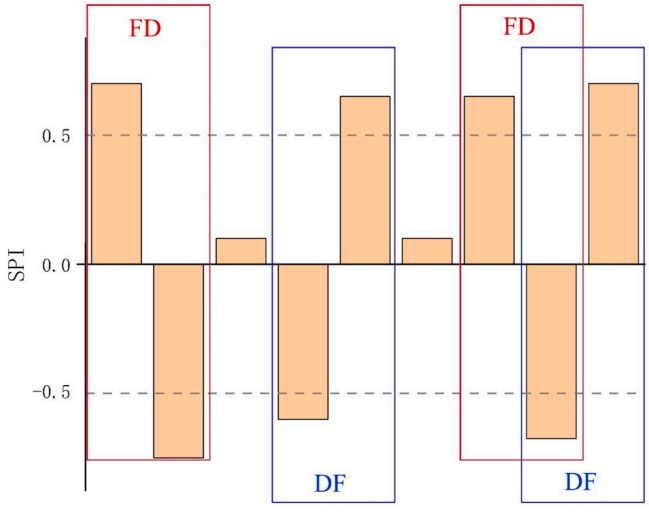

Fig. 1. Schematic diagram of DFAA event.

Table 3
Evaluation results for the different correction schemes.

	Monthly precipitation			Annual maximum monthly precipitation			Annual minimum monthly precipitation			M_s
	R	MAE (mm/month)	NRMSE	R	MAE (mm/month)	NRMSE	R	MAE (mm/month)	NRMSE	
EQM-Mean	0.856	0.643	0.728	0.878	1.400	0.477	0.739	0.198	2.576	0.528
EQM-IWM	0.852	0.639	0.736	0.862	1.237	0.432	0.681	0.157	2.239	0.528
EQM-KDE	0.704	0.959	1.087	0.778	1.531	0.526	0.540	0.120	1.726	0.153
EQM-RF	0.865	0.607	0.708	0.877	1.404	0.485	0.737	0.243	3.196	0.500
Mean-EQM	0.830	0.697	0.802	0.844	1.290	0.422	0.568	0.106	1.544	0.556
IWM-EQM	0.815	0.719	0.849	0.819	1.404	0.461	0.543	0.113	1.612	0.389
KDE-EQM	0.700	0.982	1.081	0.818	1.405	0.461	0.525	0.122	1.746	0.181
RF-EQM	0.856	0.621	0.730	0.861	1.212	0.418	0.670	0.116	1.693	0.667

a monthly precipitation fusion product under three climate scenarios (SSP126, SSP245, and SSP585) from January 2015 to December 2099. The corrected precipitation dataset based on the best correction scheme is hereinafter referred to as the RF-EQM precipitation.

4.2. *Performance evaluation of corrected precipitation based on the best correction scheme*

4.2.1. *Comparison with CN05.1 monthly precipitation*

Taking CN05.1 as the reference dataset, the monthly precipitation data before and after correction were verified. The results are shown in Fig. 2. This is a standardized Taylor plot, where the standard deviation (STD) and root mean squared difference (RMSD) are both divided by the standard deviation of the CN05.1 precipitation data. The closer the STD

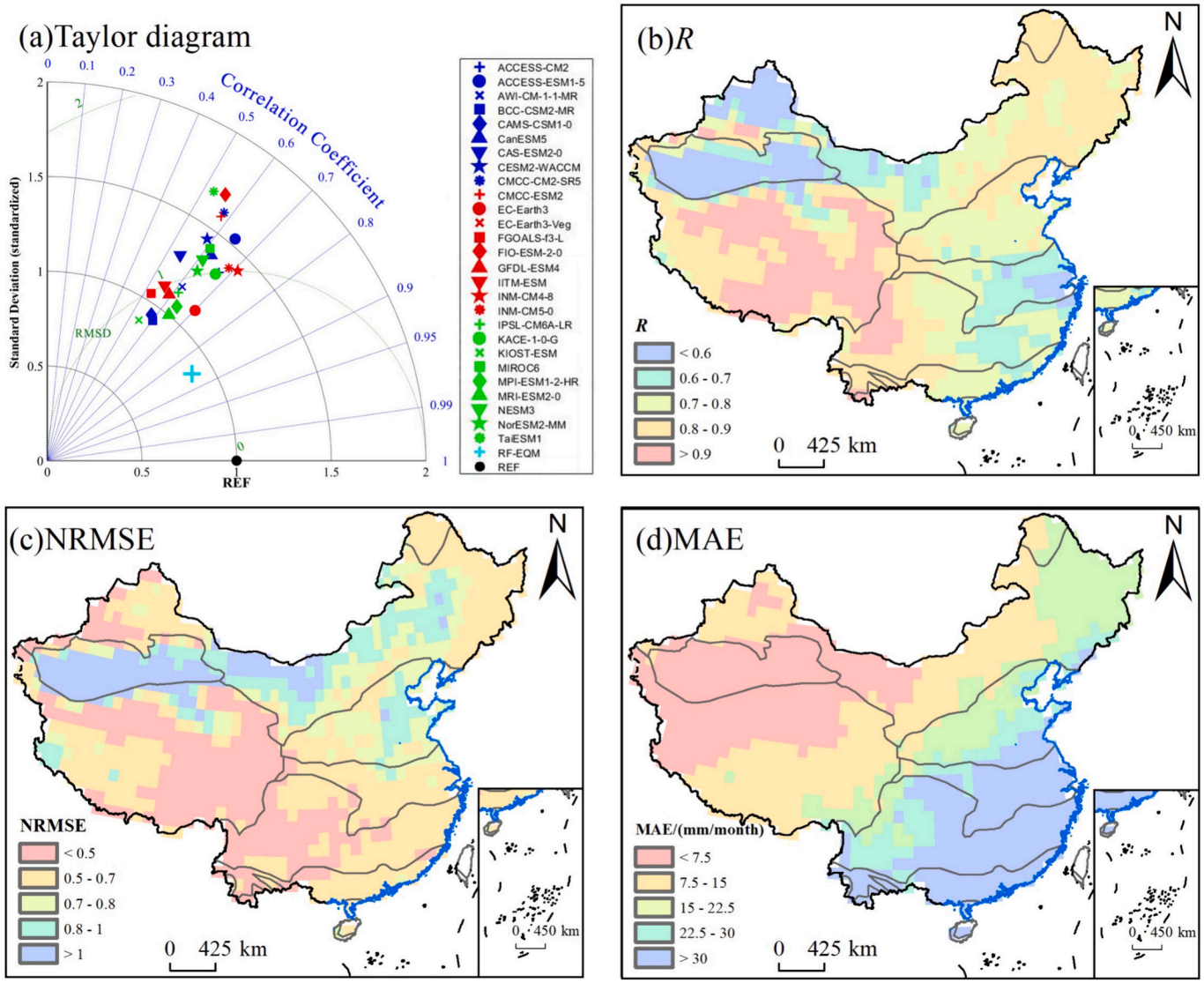

Fig. 2. Comparison of precipitation between RF-EQM and CN05.1(The research area of this paper is the mainland of China (excluding Taiwan), the same below.)

(standardized) is to 1, the better the data performs on the standard deviation indicator. The validation results show that the accuracy of the monthly precipitation was significantly improved. Before the correction, the correlation coefficients between the precipitation data simulated using the GCMs and CN05.1 were 0.526–0.708, and the correlation coefficients of only six of the 27 models were >0.65. The correlation coefficient between the corrected precipitation based on the best correction scheme (i.e., the RF-EQM precipitation) and the CN05.1 was 0.856, which was much higher than that before the correction. The RMSD (standardized) before and after the correction were 0.817–1.426 and 0.518, respectively.

There are certain spatial variations in the accuracy of the correction. The correlation coefficient between the RF-EQM and CN05.1 was the highest performance on the Qinghai-Tibet Plateau (mostly ≥0.9), followed by northeastern China (mostly between 0.8 and 0.9), and it was lower performance in northwestern China (mostly ≤0.6). The NRMSE between RF-EQM and CN05.1 is relatively low in the Qinghai Tibet Plateau region (mostly ≤0.5). The MAE values between the RF-EQM and CN05.1 increased from the northwest to the southeast coast. The calculation of MAE is affected by the size of the reference value (real value). When the relative error was the same, the greater the reference value was, the greater the absolute error of the estimated value was. The precipitation increased gradually from northwest to southeast, which may have caused the MAE between the RF-EQM and CN05.1 to increase from the northwest to the southeast coast.

4.2.2. Comparison with CN05.1 extreme precipitation

Fig. 3 presents the Taylor diagram between the extreme precipitation (annual maximum/minimum monthly precipitation) of the CN05.1 and RF-EQM. Overall, the simulation results of the annual maximum monthly precipitation are better than those of the annual minimum monthly precipitation. The RF-EQM correction greatly improved the simulation data's ability to depict extreme precipitation. According to the correlation coefficient, the R value between the annual maximum monthly precipitation (annual minimum monthly precipitation) simulated using the GCMs in the CMIP6 and the maximum (minimum) monthly precipitation of the CN05.1 before correction is between 0.745 and 0.900 (0.336–0.677), while the correlation coefficient between the annual maximum (minimum) monthly precipitation of the RF-EQM and the annual maximum (minimum) precipitation of the CN05.1 is 0.946 (0.735). From the perspective of the standard deviation, the standard deviation of the extreme monthly precipitation simulated using the CMIP6 GCMs before correction is generally large. The standard deviation (standardized) of the simulated annual minimum monthly precipitation is between 0.948– 3.290 and is generally greater than that of the simulated annual maximum monthly precipitation (0.873–1.631). The STD (standardized) of the annual maximum monthly precipitation of the RF-EQM is 0.849. The STD (standardized) of the annual minimum monthly precipitation of the RF-EQM is 1.226. According to the RMSD (standardized), the RMSD (standardized) of the annual maximum (minimum) monthly precipitation simulated using the CMIP6 GCMs before correction is 0.503–1.108 (0.954–2.795), while the RMSD (standardized) of the annual maximum (minimum) monthly precipitation of the RF-EQM and CN05.1 is 0.337 (0.837).

4.3. Comparison with ERA5 precipitation

Fig. 4 shows the Taylor diagram of the precipitation products (ERA5 and RF-EQM) and precipitation observation data (CN05.1). Regarding the monthly precipitation, the difference between the ERA5 and RF-EQM is small. The correlation coefficient between the ERA5 and CN05.1 is 0.857, which is close to the correlation coefficient between the

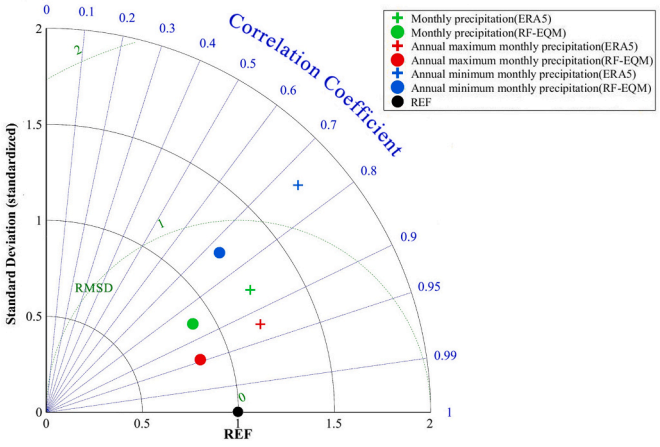

Fig. 4. Taylor diagram of precipitation products (ERA5 and RF-EQM) and precipitation observation data (CN05.1).

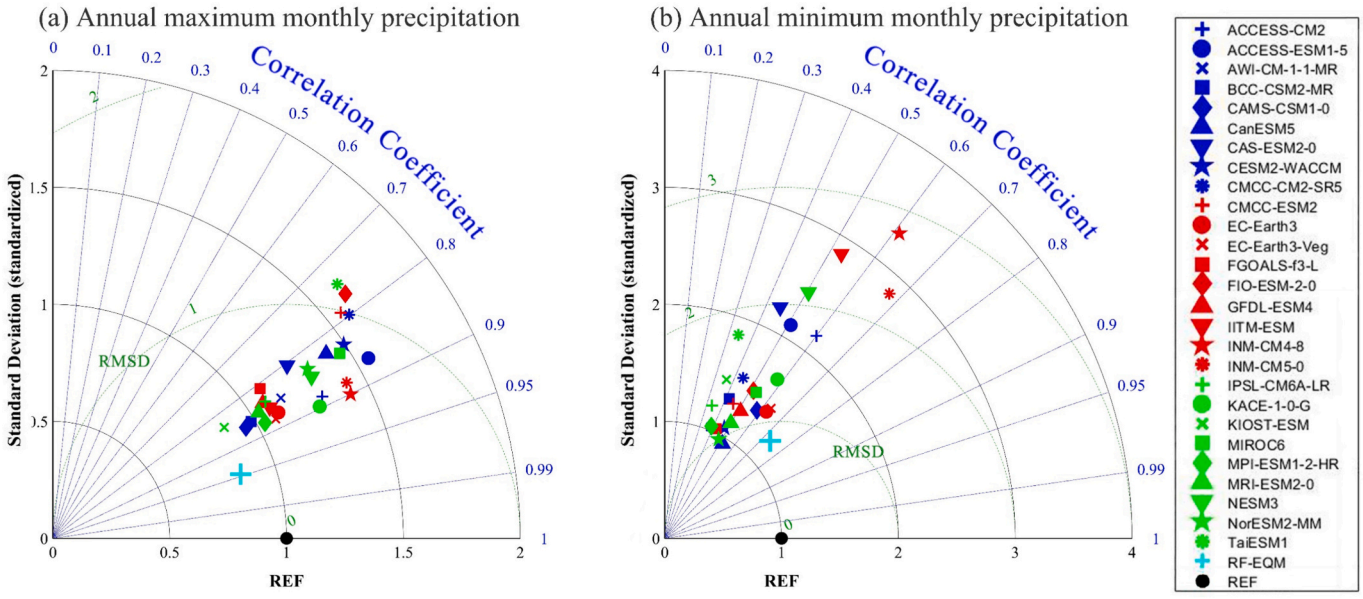

Fig. 3. Taylor diagram of CMIP6 models, RF-EQM, and reference dataset for the annual maximum precipitation and annual minimum precipitation.

RF-EQM and CN05.1 (0.856). The RMSD (standardized) between the RF-EQM and CN05.1 is 0.518, which is slightly smaller than that between the ERA5 and CN05.1 (0.640). The ERA5 overestimates the STD (standardized) of the precipitation, while the RF-EQM slightly underestimates the STD (standardized) of the precipitation. Regarding the annual extreme precipitation, the RF-EQM is significantly better than the ERA5. For the annual maximum monthly precipitation, the correlation coefficient, the RMSD (standardized), and the STD (standardized) between the ERA5 and CN05.1 are 0.925, 0.474, and 1.207, respectively; the correlation coefficient, the RMSD (standardized), and the STD (standardized) between the RF-EQM and CN05.1 are 0.947, 0.337, and 0.849, respectively. For the annual minimum monthly precipitation, the correlation coefficient, the RMSD (standardized), and the STD (standardized) between the ERA5 and CN05.1 are 0.743, 1.223, and 1.765, respectively; and the correlation coefficient, the RMSD (standardized), and the STD (standardized) between the RF-EQM and CN05.1 are 0.735, 0.837, and 1.226, respectively.

4.4. Spatiotemporal variations of alternating drought and flood events

Fig. 5 and Fig. 6 presents box plots depicting the frequencies of DF and FD events during the reference period (1995–2014) and the short-term (2021–2040), mid-term (2041–2060), and long-term (2080–2099) under the SSP126, SSP245, and SSP585 scenarios. It can be observed that in the future, the frequency of DF events is consistently increasing across all scenarios, with the SSP585 scenario exhibiting higher DF event frequencies than the other two scenarios. The median DF event frequency during the reference period is 3.05, which increases to 3.90, 4.30, and 4.60 under SSP126 scenario in the short-term, mid-term, and long-term respectively; 3.85, 4.20, and 5.15 under SSP245 scenario; and 3.95, 4.70, and 6.35 under SSP585 scenario. Compared to the historical reference period, the median DF event frequency in SSP585 during the long-term is expected to increase by 2.08 times. In contrast to DF events, the increase in FD event frequency in the future is not significant. The median FD event frequency during the reference period is 2.40, which rises to 2.65, 2.70, and 2.70 for SSP126 in the short-term, mid-term, and long-term respectively; 2.65 for SSP245 across all three terms; and 2.65, 2.65, and 2.50 for SSP585. In the long-term, unlike DF events, the median FD event frequency in SSP585 does not show an increase, but rather exhibits a slight decrease.

Fig. 7–9 illustrate the spatial distribution of the yearly frequency of historical and future DF and FD events. Overall, the frequency of DF events is higher than that of FD events during the historical period (1995–2014). The frequency of DF events is slightly higher in the Qinghai-Tibet Plateau region, while there is no significant spatial clustering of FD events (Fig. 7). In general, the frequency of DF events in the Northwestern region of China is continuously increasing in all future scenarios, while the frequency of DF events is expected to decrease in some southeastern areas (Fig. 8). Furthermore, as the events progress, the regions experiencing an increase in DF event frequency are gradually expanding, while those with a decrease in DF event frequency are shrinking. Among them, under the SSP585 long-term scenario, the increase in DF event frequency is the most significant, and the number of grids with increased DF frequency accounts for 94.88% of the total number of grids in the entire study area. Unlike DF events, FD events also exhibit an irregular spatial distribution in the future (Fig. 9). The frequency of FD events does not exhibit clustering characteristics in different scenarios or at different times, and there is no apparent regular trend in their variations.

5. Discussion

In this study, four GCM ensemble methods were used for the comparison, including the average, independent weighted mean, kernel density function, and random forest methods. we compared eight schemes for comprehensively using the EQM method and data ensemble method to conduct a precipitation bias correction:EQM-Mean , EQM-IWM , EQM-KDE , EQM-RF , Mean-EQM , IWM-EQM , KDE-EQM and RF-EQM. Base on Table 3, from the perspective of monthly precipitation, the performance of the empirical quantile mapping followed by the multi-model ensemble methods is better than that of the multi-model ensemble methods followed by empirical quantile mapping. Specifically, the R of EQM-Mean is higher than that of Mean-EQM, while MAE and NRMSE of EQM-Mean is lower than that of Mean-EQM. Similar conclusions can also be obtained from the other six methods. However, when considering the mean, maximum, and minimum values of precipitation simultaneously, the ranking of M_s for the 8 methods from largest to smallest is RF-EQM (0.667) > Mean-EQM (0.556) > EQM-Mean (0.528) = EQM-IWM (0.528) > EQM-RF (0.500) > IWM-EQM (0.389) > KDE-EQM (0.181) > EQM-KDE (0.153). This indicates different methods have different abilities in restoring the mean and extreme values of precipitation. When testing the accuracy of bias correction methods, it is not only important to consider the correction effect on monthly precipitation, but also the correction effect on extreme precipitation. Among the four ensemble methods, KDE has the worst performance. KDE is a method of estimating the probability density

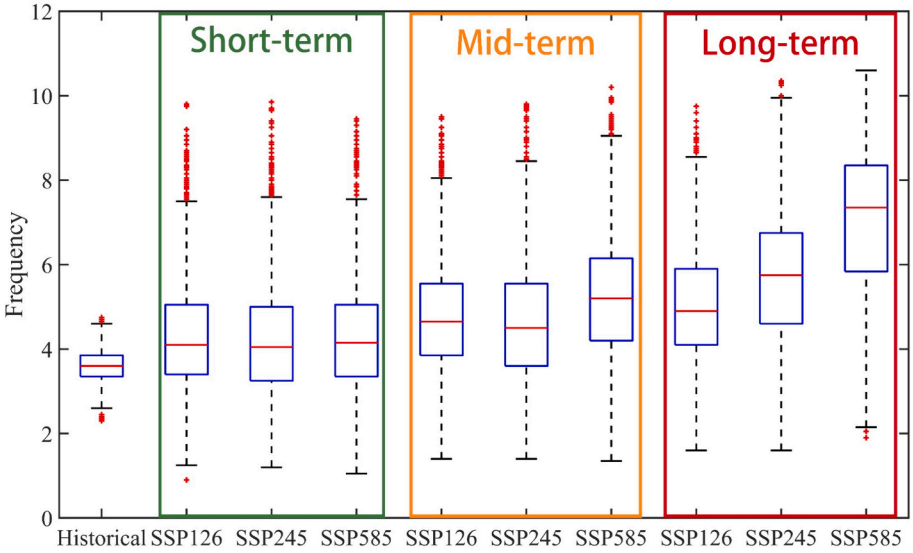

Fig. 5. The box plot of the frequency of DF events.

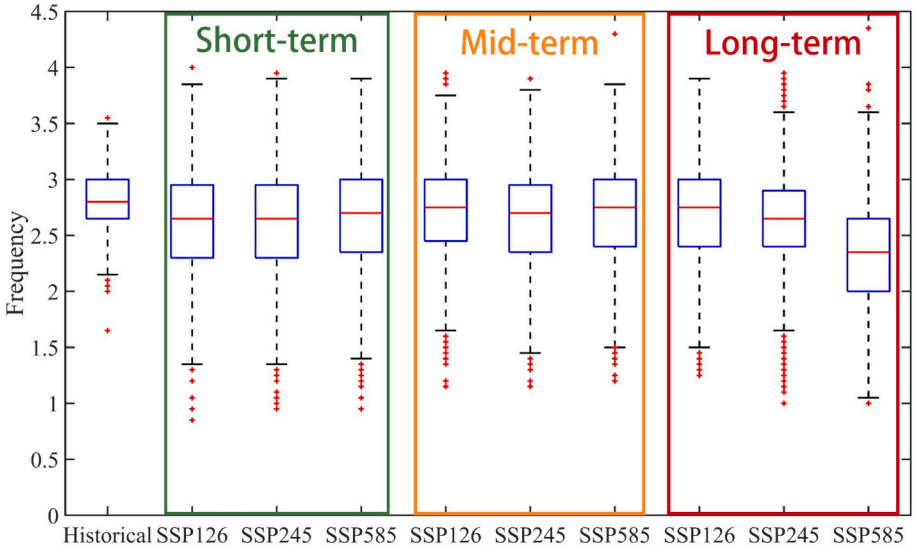

Fig. 6. The box plot of the frequency of FD events.

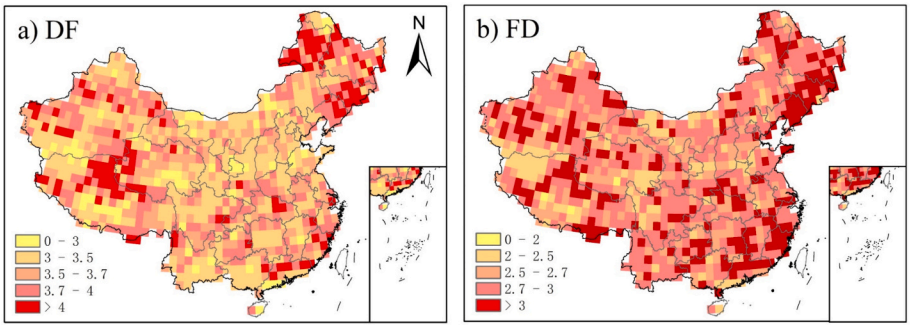

Fig. 7. The historical distribution map of the yearly frequency of DF and FD events.

function of independent and identically distributed samples through non parametric methods. For a given grid, we considered the precipitation values of 27 GCM as 27 samples, and used KDE to calculate the probability density function of precipitation, thereby obtaining the value of precipitation with the highest probability as the corrected precipitation value. This indicates that the precipitation values of the 27 models do not satisfy the assumption of independent and identically distributed. Both Mean-EQM and EQM-Mean show good correction performance which further confirms that the averaging method is feasible and the simplest method. Compared to EQM-Mean, Mean-EQM has a much smaller workload, a higher correction accuracy (Ms) and therefore more recommended to be used. EQM-RF and RF-EQM also demonstrated good correction performance, especially RF-EQM, which has the highest accuracy among all methods. RF utilizes a bootstrapping method to sample the training data, which reduces the redundancy of explanatory variables and makes the prediction model (decision tree) more diverse (He et al., 2016). This reduction in correlation among decision trees can minimize the possibility of overfitting. The overall correction effect of RF-EQM on monthly precipitation and extreme precipitation is the best. Although this study only validated and applied the RF-EQM on precipitation datasets, this method is also applicable to other climate variables, such as temperature.

Climate warming leads to changes in the water cycle, increased evaporation, and higher atmospheric water vapor content (You et al., 2022). In such conditions, on one hand, the duration of non-rainy periods may lengthen, leading to drier surface conditions during rainless periods (You et al., 2022). On the other hand, when it rains, the intensity of rainfall may also increase (You et al., 2022). Besides, DFAA events are more likely to increase both globally and regionally (Gao et al., 2022; Qiao et al., 2022; Swain et al., 2018; Zhang et al., 2021). Due to the rapid fluctuations in precipitation, vegetation may experience both water shortages and excess water in the short-term during DFAA events. This can potentially lead to ecosystem degradation and crop yield losses (Adnan et al., 2021; Huang et al., 2019; Shi et al., 2022; Zhu and Yang, 2020). This study provides predictions of future DFAA events under different emission scenarios based on a long-term (1961–2099) monthly corrected precipitation dataset with a 1° resolution. Our results indicate that the frequency of DF events will increase in all emission scenarios in the future, while the frequency of FD events shows no significant change. Therefore, we need to pay more attention to the mitigation measures for DF events. Due to different datasets or indicators used, there may be differences in the DFAA events identified by different studies. This study used a bias corrected precipitation dataset obtained by integrating 27 GCMs to identify DFAA events, theoretically reducing uncertainty.

6. Conclusions

In this study, a long-term (1961–2099) 1° resolution monthly precipitation dataset was produced, which was highly correlated with the CN05.1 data; the correlation coefficient increased from 0.526-0.708 to 0.856 after correction; the RMSE (standardized) decreased from 0.817-1.426 to 0.518 after correction. The NRMSE and MAE between the corrected precipitation and the CN05.1 were 1.176, and 0.621, respectively. Although the accuracy of the corrected extreme precipitation was lower than the accuracy of the corrected monthly precipitation, the

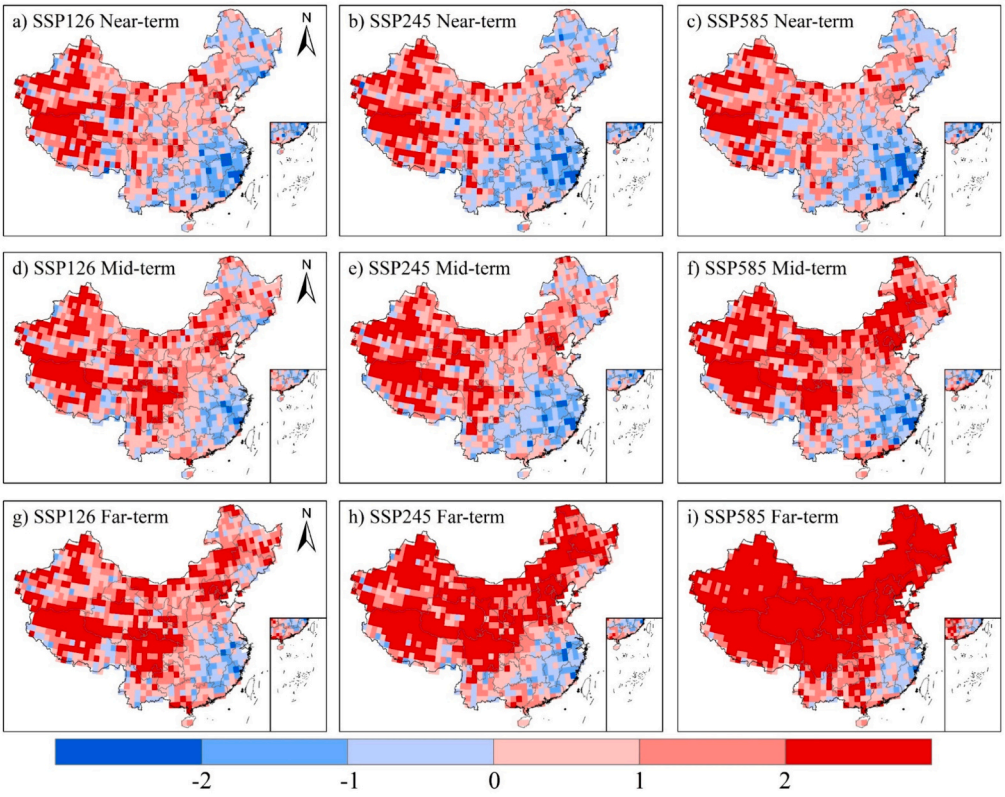

Fig. 8. Distribution of DF event yearly frequency differences between different future scenarios and historical scenarios.

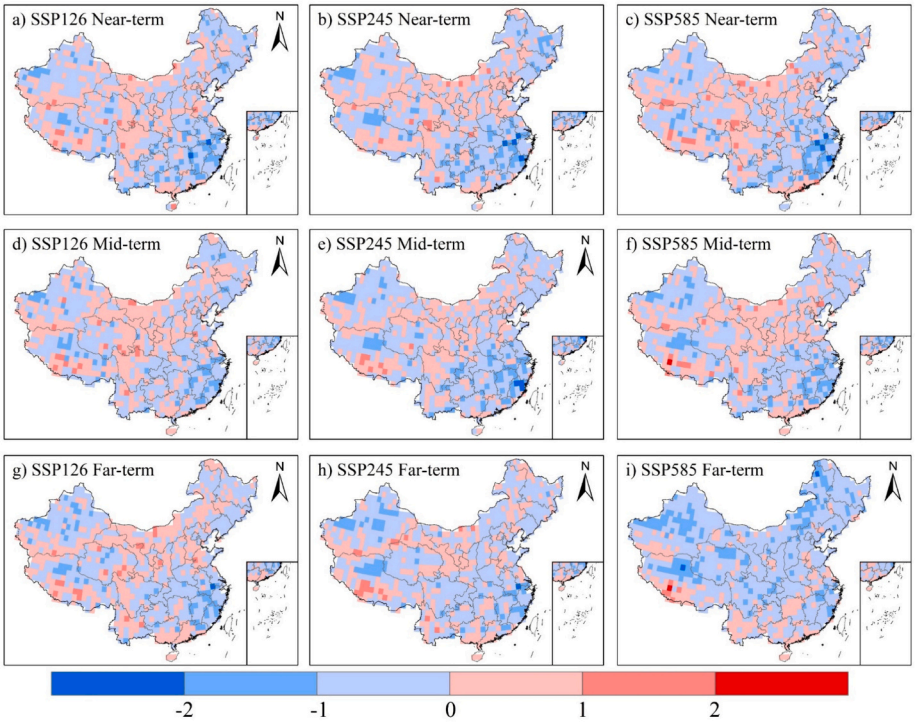

Fig. 9. Distribution of FD event yearly frequency differences between different future scenarios and historical scenarios.

accuracy of the corrected extreme precipitation was better than that of the ERA5 extreme precipitation. In addition, the overall accuracy of the corrected precipitation in the southeastern coastal region of China was lower than other region, which may be due to the large amount of precipitation in this region; the simulation effect of the GCMs was worse for high precipitation than for low precipitation. This study also utilized the produced precipitation product to project the future occurrence frequencies of DFAA events. The results indicate that the frequency of

DF events is consistently increasing across all scenarios, with the SSP585 scenario exhibiting higher DF event frequencies than the other two scenarios. Unlike DF events, the increase in FD event frequency in the future is not significant. The Qinghai-Tibet Plateau region, northeastern region, and certain areas in the northwest exhibit higher future occurrence frequencies of DF events. However, the spatial distribution of future FD event frequencies does not display noticeable clustering. This study expanded the method of bias correction of meteorological data and provided a reference for other climate parameters and precipitation bias correction in other regions. The precipitation products generated in this study could provide data support for future precipitation-related studies as well as be used as input data for dynamic downscaling models to improve the reliability of regional climate simulations in the future.

Author contributions

Tingting Liu and Xiufang Zhu worked together to set up the study idea and perform the modeling analysis. Mingxiu Tang and Chunhua Guo developed the code for the method in the study. Tingting Liu drafted the manuscript. Dongyan Lu revised the manuscript.

Disclaimer

Publisher's note: Copernicus Publications remains neutral with regard to jurisdictional claims in published maps and institutional affiliations.

CRediT authorship contribution statement

Tingting Liu: Writing – original draft, Data curation, Conceptualization. **Xiufang Zhu:** Writing – review & editing, Funding acquisition, Formal analysis, Data curation. **Mingxiu Tang:** Project administration, Methodology. **Chunhua Guo:** Software, Resources. **Dongyan Lu:** Writing – review & editing, Visualization.

Declaration of competing interest

The contact author has declared that neither of the authors has any competing interests.

Data availability

Data will be made available on request.

Acknowledgements

This work was supported by the National Natural Science Foundation of China (Grant No. 42077436), and the National Key Research and Development Program of China (Grant No. 2019YFA0606900. We thank the Institute of Atmospheric Physics, Chinese Academy of Sciences, for providing the CN05.1 dataset.

References

Adnan, R.M., Mostafa, R.R., Islam, A.R.M.T., 2021. Improving drought modeling using hybrid random vector functional link methods. Water 13, 3379.

Ahmed, K., Sachindra, D.A., Shahid, S., Iqbal, Z., Nawaz, N., Khan, N., 2020. Multi-model ensemble predictions of precipitation and temperature using machine learning algorithms. Atmos. Res. 236, 104806.

Babaousmail, H., Hou, R., Ayugi, B., Sian, K.T.C.L.K., Ojara, M., Mumo, R., Chehbouni, A., Ongoma, V., 2022. Future changes in mean and extreme precipitation over the Mediterranean and Sahara regions using bias-corrected CMIP6 models. Int. J. Climatol. 42, 7280–7297. https://doi.org/10.1002/joc.7644.

Baez-Villanueva, O.M., Zambrano-Bigiarini, M., Beck, H.E., McNamara, I., Ribbe, L., Nauditt, A., Birkel, C., Verbist, K., Giraldo-Osorio, J.D., Xuan Thinh, N., 2020. RF-MEP: a novel Random Forest method for merging gridded precipitation products and ground-based measurements. Remote Sens. Environ. 239, 111606 https://doi.org/10.1016/j.rse.2019.111606.

Bai, H., Xiao, D., Wang, B., Liu, D.L., Feng, P., Tang, J., 2021. Multi-model ensemble of CMIP6 projections for future extreme climate stress on wheat in the North China plain. Int. J. Climatol. 41, E171–E186. https://doi.org/10.1002/joc.6674.

Baran, A.A., Moglen, G.E., Godrej, A.N., 2019. Quantifying Hydrological Impacts of Climate Change Uncertainties on a Watershed in Northern Virginia.

Bishop, C.H., Abramowitz, G., 2013. Climate model dependence and the replicate Earth paradigm. Clim. Dyn. 41, 885–900. https://doi.org/10.1007/s00382-012-1610-y.

Bock, L., Lauer, A., Schlund, M., Barreiro, M., Bellouin, N., Jones, C., Meehl, G.A., Predoi, V., Roberts, M.J., Eyring, V., 2020. Quantifying progress across different CMIP phases with the ESMValTool. J. Geophys. Res. Atmos. 125 https://doi.org/10.1029/2019JD032321 e2019JD032321.

Breiman, L., 2001. Random forests. Mach. Learn. 45, 5–32. https://doi.org/10.1023/A:1010933404324.

Bruce, J.P., 1994. Natural disaster reduction and global change. Bull. Am. Meteorol. Soc. 7510 (10), 1831–1835. https://doi.org/10.1175/1520-0477(1994)075<1831:ndragc>2.0.co;2.

Cannon, A.J., 2020. Reductions in daily continental-scale atmospheric circulation biases between generations of global climate models: CMIP5 to CMIP6. Environ. Res. Lett. 15, 064006 https://doi.org/10.1088/1748-9326/ab7e4f.

Carvalho, D., Cardoso Pereira, S., Rocha, A., 2021. Future surface temperatures over Europe according to CMIP6 climate projections: an analysis with original and bias-corrected data. Clim. Chang. 167, 1–17. https://doi.org/10.1007/s10584-021-03159-0.

Chen, J., Chung, C., 2015. Representation of global precipitation anomalies using four major climate patterns. Sci. China Technol. Sci. 58, 927–934. https://doi.org/10.1007/s11431-015-5799-y.

Chen, J., Brissette, F.P., Chaumont, D., Braun, M., 2013. Finding appropriate bias correction methods in downscaling precipitation for hydrologic impact studies over North America. Water Resour. Res. 49, 4187–4205. https://doi.org/10.1002/wrcr.20331.

Chen, H., Sun, J., Lin, W., Xu, H., 2020a. Comparison of CMIP6 and CMIP5 models in simulating climate extremes. Sci. Bull. 65 https://doi.org/10.1016/j.scib.2020a.05.015.

Chen, H., Wang, S., Zhu, J., Zhang, B., 2020b. Projected changes in abrupt shifts between dry and wet extremes over China through an ensemble of regional climate model simulations. J. Geophys. Res. Atmos. 125 (23) https://doi.org/10.1029/2020jd033894.

Chen, C.-A., Hsu, H.-H., Liang, H.-C., 2021. Evaluation and comparison of CMIP6 and CMIP5 model performance in simulating the seasonal extreme precipitation in the Western North Pacific and East Asia. Weather Clim. Extrem. 31, 100303 https://doi.org/10.1016/j.wace.2021.100303.

Colette, A., Vautard, R., Vrac, M., 2012. Regional climate downscaling with prior statistical correction of the global climate forcing. Geophys. Res. Lett. 39 https://doi.org/10.1029/2012GL052258.

Déqué, M., 2007. Frequency of precipitation and temperature extremes over France in an anthropogenic scenario: model results and statistical correction according to observed values. Glob. Planet. Chang. 57, 16–26. https://doi.org/10.1016/j.gloplacha.2006.11.030.

Dey, A., Sahoo, D.P., Kumar, R., Remesan, R., 2022. A multimodel ensemble machine learning approach for CMIP6 climate model projections in an Indian River basin. Int. J. Climatol. 42 (16), 9215–9236.

Dike, V.N., Lin, Z., Fei, K., Langendijk, G.S., Nath, D., 2022. Evaluation and multimodel projection of seasonal precipitation extremes over Central Asia based on CMIP6 simulations. Int. J. Climatol. 42, 7228–7251. https://doi.org/10.1002/joc.7641.

Dong, S., Xu, Y., Zhou, B., Shi, Y., 2015. Assessment of indices of temperature extremes simulated by multiple CMIP5 models over China. Adv. Atmos. Sci. 32, 1077–1091. https://doi.org/10.1007/s00376-015-4152-5.

Duda, R., Hart, P., Stork, G., D., 2001. Pattern Classification. Wiley Interscience.

Fernandez-Granja, J.A., Casanueva, A., Bedia, J., Fernandez, J., 2021. Improved atmospheric circulation over Europe by the new generation of CMIP6 earth system models. Clim. Dyn. 56, 3527–3540. https://doi.org/10.1007/s00382-021-05652-9.

Fu, G., Charles, S.P., Kirshner, S., 2013. Daily rainfall projections from general circulation models with a downscaling nonhomogeneous hidden Markov model (NHMM) for South-Eastern Australia. Hydrol. Process. 27, 3663–3673. https://doi.org/10.1002/hyp.9483.

Gao, X., Zhao, D., Chen, Z., Zhu, Y., 2022. Changes in abrupt alternations between wet and dry over the Great Lakes Region of Central Asia during the period 1976–2015. J. Hydrol. 613, 128333.

Gat, J.R., Airey, P.L., 2006. Stable water isotopes in the atmosphere/biosphere/lithosphere interface: scaling-up from the local to continental scale, under humid and dry conditions. Glob. Planet. Chang. 51, 25–33. https://doi.org/10.1016/j.gloplacha.2005.12.004.

Gudmundsson, L., Bremnes, J.B., Haugen, J.E., Engen-Skaugen, T., 2012. Technical note: Downscaling RCM precipitation to the station scale using statistical transformations – a comparison of methods. Hydrol. Earth Syst. Sci. 16, 3383–3390. https://doi.org/10.5194/hess-16-3383-2012.

Guo, H., Bao, A., Chen, T., Zheng, G., Wang, Y., Jiang, L., De Maeyer, P., 2021. Assessment of CMIP6 in simulating precipitation over arid Central Asia. Atmos. Res. 252, 105451 https://doi.org/10.1016/j.atmosres.2021.105451.

Gusain, A., Ghosh, S., Karmakar, S., 2020. Added value of CMIP6 over CMIP5 models in simulating Indian summer monsoon rainfall. Atmos. Res. 232, 104680 https://doi.org/10.1016/j.atmosres.2019.104680.

Harvey, B.J., Cook, P., Shaffrey, L.C., Schiemann, R., 2020. The response of the Northern Hemisphere storm tracks and Jet Streams to climate change in the CMIP3, CMIP5, and CMIP6 climate models. J. Geophys. Res. Atmos. 125 https://doi.org/10.1029/2020JD032701 e2020JD032701.

He, B., Bao, Q., Wang, X., Zhou, L., Wu, X., Liu, Y., Wu, G., Chen, K., He, S., Hu, W., Li, J., Li, J., Nian, G., Wang, L., Yang, J., Zhang, M., Zhang, X., 2019. CAS FGOALS-f3-L model datasets for CMIP6 historical atmospheric model intercomparison project simulation. Adv. Atmos. Sci. 36, 771–778. https://doi.org/10.1007/s00376-019-9027-8.

He, X., Chaney, N.W., Schleiss, M., Sheffield, J., 2016. Spatial downscaling of precipitation using adaptable random forests. Water Resour. Res. 52 (10), 8217–8237.

Held, I.M., Soden, B.J., 2006. Robust responses of the hydrological cycle to global warming. J. Clim. 19, 5686–5699. https://doi.org/10.1175/JCLI3990.1.

Huang, J., Hu, T., Yasir, M., Gao, Y., Chen, C., Zhu, R., Yang, J., 2019. Root growth dynamics and yield responses of rice (Oryza sativa L.) under drought—Flood abrupt alternating conditions. Environ. Exp. Bot. 157, 11–25.

Huang, A., Zhou, Y., Zhang, Y., Huang, D., Zhao, Y., Wu, H., 2014. Changes of the annual precipitation over Central Asia in the twenty-first century projected by multimodels of CMIP5. J. Clim. 27, 6627–6646. https://doi.org/10.1175/JCLI-D-14-00070.1.

Jiang, J., Zhou, T., 2021. Human-induced rainfall reduction in drought-prone Northern Central Asia. Geophys. Res. Lett. 48 https://doi.org/10.1029/2020GL092156 e2020GL092156.

Jiang, D., Hu, D., Tian, Z., Lang, X., 2020a. Differences between CMIP6 and CMIP5 models in simulating climate over China and the East Asian Monsoon. Adv. Atmos. Sci. 37, 1102–1118. https://doi.org/10.1007/s00376-020-2034-y.

Jiang, J., Zhou, T., Chen, X., Zhang, L., 2020b. Future changes in precipitation over Central Asia based on CMIP6 projections. Environ. Res. Lett. 15, 054009 https://doi.org/10.1088/1748-9326/ab7d03.

Jiao, D., Xu, N., Yang, F., Xu, K., 2021. Evaluation of spatial-temporal variation performance of ERA5 precipitation data in China. Sci. Rep. 11 (1), 17956.

Jose, D.M., Dwarakish, G.S., 2022. Bias correction and trend analysis of temperature data by a high-resolution CMIP6 model over a tropical river basin. Asia-Pac. J. Atmos. Sci. 58, 97–115. https://doi.org/10.1007/s13143-021-00240-7.

Jose, D.M., Vincent, A.M., Dwarakish, G.S., 2022. Improving multiple model ensemble predictions of daily precipitation and temperature through machine learning techniques. Sci. Rep. 12 (1), 4678.

Kukulies, J., Chen, D., Wang, M., 2020. Temporal and spatial variations of convection, clouds and precipitation over the Tibetan Plateau from recent satellite observations. Part II: precipitation climatology derived from global precipitation measurement mission. Int. J. Climatol. 40, 4858–4875. https://doi.org/10.1002/joc.6493.

Li, H., Sheffield, J., Wood, E.F., 2010. Bias correction of monthly precipitation and temperature fields from Intergovernmental Panel on Climate Change AR4 models using equidistant quantile matching. J. Geophys. Res. Atmos. 115 https://doi.org/10.1029/2009JD012882.

Li, L., She, D., Zheng, H., Lin, P., Yang, Z.-L., 2020a. Elucidating diverse drought characteristics from two Meteorological Drought Indices (SPI and SPEI) in China. J. Hydrometeorol. 21, 1513–1530. https://doi.org/10.1175/JHM-D-19-0290.1.

Li, S.-Y., Miao, L.-J., Jiang, Z.-H., Wang, G.-J., Gnyawali, K.R., Zhang, J., Zhang, H., Fang, K., He, Y., Li, C., 2020b. Projected drought conditions in Northwest China with CMIP6 models under combined SSPs and RCPs for 2015–2099. Adv. Clim. Chang. Res. 11, 210–217. https://doi.org/10.1016/j.accre.2020.09.003.

Li, T., Jiang, Z., Le Treut, H., Li, L., Zhao, L., Ge, L., 2021a. Machine learning to optimize climate projection over China with multi-model ensemble simulations. Environ. Res. Lett. 16 (9), 094028.

Li, Y., Yan, D., Peng, H., Xiao, S., 2021b. Evaluation of precipitation in CMIP6 over the Yangtze River Basin. Atmos. Res. 253, 105406 https://doi.org/10.1016/j.atmosres.2020.105406.

Lim Kam Sian, K.T.C., Hagan, D.F.T., Ayugi, B.O., Nooni, I.K., Ullah, W., Babaousmail, H., Ongoma, V., 2022. Projections of precipitation extremes based on bias-corrected coupled Model Intercomparison Project phase 6 models ensemble over southern Africa. Int. J. Climatol. https://doi.org/10.1002/joc.7707.

Lovino, M.A., Pierrestegui, M.J., Müller, O.V., Berbery, E.H., Müller, G.V., Pasten, M., 2021. Evaluation of historical CMIP6 model simulations and future projections of temperature and precipitation in Paraguay. Clim. Chang. 164, 46. https://doi.org/10.1007/s10584-021-03012-4.

McKee, T. B., Doesken, N. J., Kleist, J., 1993. The relationship of drought frequency and duration to time scales. Paper presented at the Proceedings of the 8th Conference on Applied Climatology.

Michelson, D.B., 2004. Systematic correction of precipitation gauge observations using analyzed meteorological variables. J. Hydrol. 290, 161–177. https://doi.org/10.1016/j.jhydrol.2003.10.005.

Mondal, S.K., Huang, J., Wang, Y., Su, B., Zhai, J., Tao, H., Wang, G., Fischer, T., Wen, S., Jiang, T., 2021. Doubling of the population exposed to drought over South Asia: CMIP6 multi-model-based analysis. Sci. Total Environ. 771, 145186 https://doi.org/10.1016/j.scitotenv.2021.145186.

Morin, E., Marra, F., Armon, M., 2020. Dryland precipitation climatology from satellite observations. In: Levizzani, V., Kidd, C., Kirschbaum, D.B., Kummerow, C.D., Nakamura, K., Turk, F.J. (Eds.), Satellite Precipitation Measurement: Volume 2. Springer International Publishing, Cham, pp. 843–859. https://doi.org/10.1007/978-3-030-35798-6_19.

Mukhamedjanov, S., Mukhomedjanov, A., Sagdullaev, R., Khasanova, N., 2021. Adaptation to climate change in irrigated agriculture in Uzbekistan. Irrig. Drain. 70, 169–176. https://doi.org/10.1002/ird.2529.

New, M., Lister, D., Hulme, M., Makin, I., 2002. A high-resolution data set of surface climate over global land areas. Clim. Res. 21, 1–25. https://doi.org/10.3354/cr021001.

Niu, J., Chen, J., Wang, K., Sivakumar, B., 2017. Coherent modes in multi-scale variability of precipitation over the headwater catchments in the Pearl River basin, South China. Hydrol. Process. 31, 948–955. https://doi.org/10.1002/hyp.11078.

Oruc, S., 2022. Performance of bias corrected monthly CMIP6 climate projections with different reference period data in Turkey. Acta Geophys. 70, 777–789. https://doi.org/10.1007/s11600-022-00731-9.

Piao, J., Chen, W., Wang, L., Chen, S., 2022. Future projections of precipitation, surface temperatures and drought events over the monsoon transitional zone in China from bias-corrected CMIP6 models. Int. J. Climatol. 42, 1203–1219. https://doi.org/10.1002/joc.7297.

Qiao, Y., Xu, W., Meng, C., Liao, X., Qin, L., 2022. Increasingly dry/wet abrupt alternation events in a warmer world: Observed evidence from China during 1980–2019. Int. J. Climatol. 42 (12), 6429–6440.

Sachindra, D.A., Huang, F., Barton, A., Perera, B.J.C., 2014. Statistical downscaling of general circulation model outputs to precipitation—part 2: bias-correction and future projections. Int. J. Climatol. 34, 3282–3303. https://doi.org/10.1002/joc.3915.

Schuenemann, K.C., Cassano, J.J., 2009. Changes in synoptic weather patterns and Greenland precipitation in the 20th and 21st centuries: 1. Evaluation of late 20th century simulations from IPCC models. J. Geophys. Res. Atmos. 114 https://doi.org/10.1029/2009JD011705.

Scott, D.W., 1992. Multivariate Density Estimation. Wiley-Interscience, New York.

Seo, S.N., Mendelsohn, R., 2008. Animal husbandry in Africa: Climate change impacts and adaptations. Afr. J. Agric. Resour. Econ. https://doi.org/10.22004/ag.econ.56968.

Shan, L., Zhang, L., Xiong, Z., Chen, X., Chen, S., Yang, W., 2018. Spatio-temporal evolution characteristics and prediction of dry–wet abrupt alternation during the summer monsoon in the middle and lower reaches of the Yangtze River Basin. Meteorol. Atmos. Phys. 130 (4), 427–440. https://doi.org/10.1007/s00703-017-0528-7.

Sheather, S.J., 2004. Density estimation. Stat. Sci. 19, 588–597.

Shetty, S., Umesh, P., Shetty, A., 2023. The effectiveness of machine learning-based multi-model ensemble predictions of CMIP6 in Western Ghats of India. Int. J. Climatol. 43 (11), 5029–5054.

Shi, W., Huang, S., Liu, D., Huang, Q., Han, Z., Leng, G., Wang, H., Liang, H., Li, P., Wei, X., 2021. Drought-flood abrupt alternation dynamics and their potential driving forces in a changing environment. J. Hydrol. 597, 126179. https://doi.org/10.1016/j.jhydrol.2021.126179.

Shi, W., Huang, S., Zhang, K., Liu, B., Liu, D., Huang, Q., Chao, L., 2022. Quantifying the superimposed effects of drought-flood abrupt alternation stress on vegetation dynamics of the Wei River Basin in China. J. Hydrol. 612, 128105.

Shrestha, A., Rahaman, M.M., Kalra, A., Jogineedi, R., Maheshwari, P., 2020. Climatological drought forecasting using bias corrected CMIP6 climate data: a case study for India. Forecasting 2, 59–84. https://doi.org/10.3390/forecast2020004.

Song, Z., Xia, J., She, D., Li, L., Hu, C., Hong, S., 2021. Assessment of meteorological drought change in the 21st century based on CMIP6 multi-model ensemble projections over mainland China. J. Hydrol. 601, 126643 https://doi.org/10.1016/j.jhydrol.2021.126643.

Song, Y.H., Chung, E.-S., Shahid, S., 2022. Uncertainties in evapotranspiration projections associated with estimation methods and CMIP6 GCMs for South Korea. Sci. Total Environ. 825, 153953 https://doi.org/10.1016/j.scitotenv.2022.153953.

Supharatid, S., Nafung, J., Aribarg, T., 2021. Projected changes in temperature and precipitation over mainland Southeast Asia by CMIP6 models. J. Water Clim. Chang. 13, 337–356. https://doi.org/10.2166/wcc.2021.015.

Supharatid, S., Aribarg, T., Nafung, J., 2022. Bias-corrected CMIP6 climate model projection over Southeast Asia. Theor. Appl. Climatol. 147, 669–690. https://doi.org/10.1007/s00704-021-03844-1.

Swain, D.L., Langenbrunner, B., Neelin, J.D., Hall, A., 2018. Increasing precipitation volatility in twenty-first-century California. Nat. Clim. Chang. 8, 427–433.

Ta, Z., Yu, Y., Sun, L., Chen, X., Mu, G., Yu, R., 2018. Assessment of precipitation simulations in Central Asia by CMIP5 climate models. Water 10, 1516. https://doi.org/10.3390/w10111516.

Tabari, H., 2020. Climate change impact on flood and extreme precipitation increases with water availability. Sci. Rep. 10, 13768. https://doi.org/10.1038/s41598-020-70816-2.

Taylor, K.E., Stouffer, R.J., Meehl, G.A., 2012. An overview of CMIP5 and the experiment design. Bull. Am. Meteorol. Soc. 93, 485–498. https://doi.org/10.1175/BAMS-D-11-00094.1.

Wang, L., Chen, W., 2014. A CMIP5 multimodel projection of future temperature, precipitation, and climatological drought in China. Int. J. Climatol. 34, 2059–2078. https://doi.org/10.1002/joc.3822.

Wang, B., Zheng, L., Liu, D.L., Ji, F., Clark, A., Yu, Q., 2018. Using multi-model ensembles of CMIP5 global climate models to reproduce observed monthly rainfall and temperature with machine learning methods in Australia. Int. J. Climatol. 38 (13), 4891–4902.

Wang, B., Jin, C., Liu, J., 2020. Understanding future change of global monsoons projected by CMIP6 models. J. Clim. 33, 6471–6489. https://doi.org/10.1175/JCLI-D-19-0993.1.

Wang, Y.R., Hessen, D.O., Samset, B.H., Stordal, F., 2022. Evaluating global and regional land warming trends in the past decades with both MODIS and ERA5-land land surface temperature data. Remote Sens. Environ. 280, 113181.

Wei, L., Jiheng, L., Junhong, G., Zhe, B., Lingbo, F., Baodeng, H., 2020. The effect of precipitation on hydropower generation capacity: a perspective of climate change. Front. Earth Sci. 8:268.DOI:10.3389/feart.2020.00268..

White, R.H., Toumi, R., 2013. The limitations of bias correcting regional climate model inputs. Geophys. Res. Lett. 40, 2907–2912. https://doi.org/10.1002/grl.50612.

Wu, J., Gao, X., 2013. A gridded daily observation dataset over China region and comparison with the other datasets. Chin. J. Geophys. 56, 1102–1111.

Wu, Z., Li, J., He, J., Jiang, Z., 2006. Large-scale atmospheric singularities and summer long-cycle droughts-floods abrupt alternation in the middle and lower reaches of the Yangtze River. Chin. Sci. Bull. 51 (16), 2027–2034. https://doi.org/10.1007/s11434-006-2060-x.

Wu, T., Lu, Y., Fang, Y., Xin, X., Li, L., Li, W., Jie, W., Zhang, J., Liu, Y., Zhang, L., Zhang, F., Zhang, Y., Wu, F., Li, J., Chu, M., Wang, Z., Shi, X., Liu, X., Wei, M., Huang, A., Zhang, Y., Liu, X., 2019. The Beijing Climate Center Climate System Model (BCC-CSM): the main progress from CMIP5 to CMIP6. Geosci. Model Dev. 12, 1573–1600. https://doi.org/10.5194/gmd-12-1573-2019.

Xiang, Y., Wang, Y., Chen, Y., Zhang, Q., 2022. Impact of climate change on the hydrological regime of the Yarkant River Basin, China: an assessment using three SSP scenarios of CMIP6 GCMs. Remote Sens. 14, 115. https://doi.org/10.3390/rs14010115.

Xie, P., Chen, M., Yang, S., Yatagai, A., Hayasaka, T., Fukushima, Y., Liu, C., 2007. A Gauge-based analysis of daily precipitation over East Asia. J. Hydrometeorol. 8, 607–626. https://doi.org/10.1175/JHM583.1.

Xin, X., Wu, T., Zhang, J., Yao, J., Fang, Y., 2020. Comparison of CMIP6 and CMIP5 simulations of precipitation in China and the East Asian summer monsoon. Int. J. Climatol. 40, 6423–6440. https://doi.org/10.1002/joc.6590.

Xu, Y., Zhang, X., Hao, Z., Hao, F., Li, C., 2021. Projections of future meteorological droughts in China under CMIP6 from a three-dimensional perspective. Agric. Water Manag. 252, 106849 https://doi.org/10.1016/j.agwat.2021.106849.

Yang, X., Wood, E.F., Sheffield, J., Ren, L., Zhang, M., Wang, Y., 2018. Bias correction of historical and future simulations of precipitation and temperature for China from CMIP5 models. J. Hydrometeorol. 19, 609–623. https://doi.org/10.1175/JHM-D-17-0180.1.

Yang, C., Bo-Tao, Z., Zhen-Yu, H. a N., Ying, X.U., 2020. Evaluation of multi-RegCM4 dynamical downscaling simulations on cluster high temperature events in China. Adv. Clim. Chang. Res. 16, 657. https://doi.org/10.12006/j.issn.1673-1719.2019.226.

Yang, J., Xiang, Y., Sun, J., Xu, X., 2022. Multi-model ensemble prediction of summer precipitation in China based on machine learning algorithms. Atmosphere 13 (9), 1424.

Yao, J., Chen, Y., Chen, J., Zhao, Y., Tuoliewubieke, D., Li, J., Yang, L., Mao, W., 2021. Intensification of extreme precipitation in arid Central Asia. J. Hydrol. 598, 125760 https://doi.org/10.1016/j.jhydrol.2020.125760.

Yi-Yang, H.U., Ying, X.U., Jin-Jian, L.I., Zhen-Yu, H. a N., 2021. Evaluation on the performance of CMIP6 global climate models with different horizontal resolution in simulating the precipitation over China. Adv. Clim. Chang. Res. 17, 730. https://doi.org/10.12006/j.issn.1673-1719.2021.005.

You, Q., Cai, Z., Wu, F., Jiang, Z., Pepin, N., Shen, S.S.P., 2021. Temperature dataset of CMIP6 models over China: evaluation, trend and uncertainty. Clim. Dyn. 57, 17–35. https://doi.org/10.1007/s00382-021-05691-2.

You, Q.L., Jiang, Z.H., Yue, X., 2022. Recent frontiers of climate changes in East Asia at global warming of 1.5 C and 2 C. Npj. Clim. Atmos Sci 5, 1–17.

Yue, Y., Yan, D., Yue, Q., Ji, G., Wang, Z., 2021. Future changes in precipitation and temperature over the Yangtze River Basin in China based on CMIP6 GCMs. Atmos. Res. 264, 105828 https://doi.org/10.1016/j.atmosres.2021.105828.

Zarrin, A., Dadashi-Roudbari, A., 2021. Projection of future extreme precipitation in Iran based on CMIP6 multi-model ensemble. Theor. Appl. Climatol. 144, 643–660. https://doi.org/10.1007/s00704-021-03568-2.

Zarrin, A., Dadashi-Roudbari, A., Hassani, S., 2022. Future changes in precipitation extremes over Iran: insight from a CMIP6 bias-corrected multi-model ensemble. Pure Appl. Geophys. 179, 441–464. https://doi.org/10.1007/s00024-021-02904-x.

Zhang, B., Wang, S., Zscheischler, J., 2021. Higher probability of abrupt shift from drought to heavy rainfall in a warmer world. doi: 10.21203/rs.3.rs-940109/v1.

Zhou, Y., Ma, Z., Wang, L., 2002. Chaotic dynamics of the flood series in the Huaihe River Basin for the last 500 years. J. Hydrol. 258 (1–4), 100–110. https://doi.org/10.1016/s0022-1694(01)00561-3.

Zhu, X., Ji, Z., Wen, X., Lee, S.-Y., Wei, Z., Zheng, Z., Dong, W., 2021. Historical and projected climate change over three major river basins in China from Fifth and Sixth Coupled Model Intercomparison Project models. Int. J. Climatol. 41, 6455–6473. https://doi.org/10.1002/joc.7206.

Zhu, H., Jiang, Z., Li, J., Li, W., Sun, C., Li, L., 2020. Does CMIP6 inspire more confidence in simulating climate extremes over China? Adv. Atmos. Sci. 37, 1119–1132. https://doi.org/10.1007/s00376-020-9289-1.

Zhu, Y.-Y., Yang, S., 2020. Evaluation of CMIP6 for historical temperature and precipitation over the Tibetan Plateau and its comparison with CMIP5. Adv. Clim. Chang. Res. 11, 239–251. https://doi.org/10.1016/j.accre.2020.08.001.

Zou, J., Lu, N., Jiang, H., Qin, J., Yao, L., Xin, Y., Su, F., 2022. Performance of air temperature from ERA5-Land reanalysis in coastal urban agglomeration of Southeast China. Sci. Total Environ. 828, 154459.